analytical chemistry

Article

Cite This: *Anal. Chem.* 2018, 90, 9888−9896

pubs.acs.org/ac

Multiplexed Instrument-Free Bar-Chart SpinChip Integrated with Nanoparticle-Mediated Magnetic Aptasensors for Visual Quantitative Detection of Multiple Pathogens

Xiaofeng Wei,[†] Wan Zhou,[†] Sharma T. Sanjay,[†] Jie Zhang,[†] Qijie Jin,[†,▽] Feng Xu,[○] Delfina C. Dominguez,[‡] and XiuJun Li*[,†,§,∥,#]

[†]Department of Chemistry and Biochemistry, [‡]College of Health Sciences, [§]Biomedical Engineering, [∥]Border Biomedical Research Center, and [#]Environmental Science and Engineering, University of Texas at El Paso, 500 West University Avenue, El Paso, Texas 79968, United States

[▽]College of Materials Science and Engineering, Nanjing Tech University, Nanjing, 210009, People's Republic of China

[○]Bioinspired Engineering and Biomechanics Center, Xi'an Jiaotong University, Xi'an, 710049, People's Republic of China

Supporting Information

ABSTRACT: A portable multiplexed bar-chart SpinChip (MB-SpinChip) integrated with nanoparticle-mediated magnetic aptasensors was developed for visual quantitative instrument-free detection of multiple pathogens. This versatile multiplexed SpinChip combines aptamer-specific recognition and nanoparticle-catalyzed pressure amplification to achieve a sample-to-answer output for sensitive point-of-care testing (POCT). This is the first report of pathogen detection using a volumetric bar-chart chip, and it is also the first bar-chart chip using a "spinning" mechanism to achieve multiplexed bar-chart detection. Additionally, the introduction of the spin unit not only enabled convenient sample introduction from one inlet to multiple separate channels in the multiplexed detection, but also elegantly solved the pressure cross-interference problem in the multiplexed volumetric bar-chart chip. This user-friendly MB-SpinChip allows visual quantitative detection of multiple pathogens simultaneously with high sensitivity but without utilizing any specialized instruments. Using this MB-SpinChip, three major foodborne pathogens including *Salmonella enterica*, *Escherichia coli*, and *Listeria monocytogenes* were specifically quantified in apple juice with limits of detection of about 10 CFU/mL. This MB-SpinChip with a bar-chart-based visual quantitative readout has great potential for the rapid simultaneous detection of various pathogens at the point of care and wide applications in food safety, environmental surveillance, and infectious disease diagnosis.

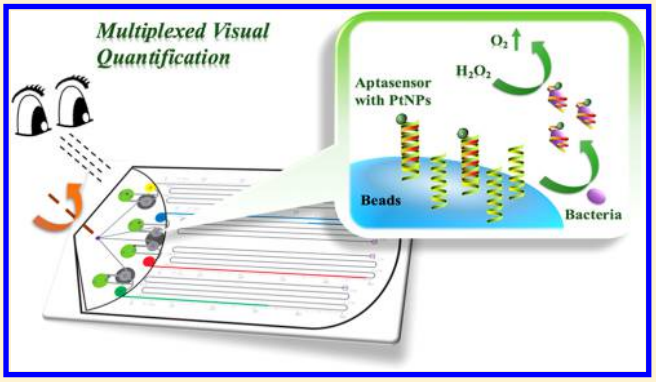

Numerous laboratory detection techniques have been developed and standardized for various applications such as food safety surveillance and diagnosis of infectious diseases caused by pathogens. For instance, as reported by the World Health Organization (WHO), each year almost 1 in 10 people (estimated 600 million globally) get ill after orally taking unsafe food, and 420 000 die in the world.[1] To monitor food safety and infectious diseases, multiple instrumental analysis methods including fluorescence,[2−4] electrochemistry,[5−7] colorimetry,[8−10] surface-enhanced Raman scattering (SERS),[11,12] and chromatography[13] have been developed for pathogen identification and quantification. However, those methods require costly and cumbersome instruments, moderate laboratory conditions, sophisticated operations, and well-trained professional personnel. Those factors become major roadblocks for these conventional methods to be employed to provide timely monitoring of pathogens on site and in low-resource settings such as developing nations. As per the ASSURED criteria from WHO,[14] the point-of-care testing (POCT) should be advocated to be affordable, sensitive, specific, user-friendly, rapid and robust, equipment-free, and deliverable to end users especially in the developing countries or resource-limited regions. Therefore, the development of cost-effective, user-friendly, and quantitative POC methods is in great need.

Over past decades, considerable microfluidic POCTs have been employed to meet the challenges and requirements. First, some hand-held devices or cellphone-assistant platforms were built to achieve the low-cost portable detection. Several photothermal,[15] colorimetric,[16−20] glucose-metric,[21−24] pressure-metric,[25−27] centrifuge-based,[28,29] and camera-based[30,31] systems were proposed to displace expensive instruments with

Received: May 8, 2018
Accepted: July 20, 2018
Published: July 20, 2018

DOI: 10.1021/acs.analchem.8b02055
Anal. Chem. 2018, 90, 9888−9896

frequently used portable devices, such as a thermometer, cellphone, glucometer, and barometer, etc. For example, Li's group developed a novel photothermal biomolecular quantitation method using a common thermometer as the quantitative signal reader.[15,32] The nanoparticle-mediated photothermal effect was first introduced in immunoassays for quantitation of various disease biomarkers and proteins, achieving a low-cost, portable, and quantitative readout method for nonprofessional people. Although reducing the cost in instrumentation with those frequently used portable detectors, low-degree integration and accessary readout detectors still limit the development and application of related methods in remote regions. Real equipment-free setup requires neither an excitation source, such as light or electricity, nor an additional signal detector, which are hard to be concurrently fulfilled in POCTs. Second, due to the low-cost nature of paper, a hot research field was focused on paper-based platforms to develop a series of instrument-free analytical methods, such as colorimetric,[33−35] time-based,[36−38] and counter-based[39,40] paper-based microfluidic devices. Many features including reagent storage, filtration, reaction incubation, and capillary driving have been integrated on paper-based microfluidic devices. However, concessive sensitivity and low throughput restrict the paper-based POCTs' generality and detection sensitivity. For instance, colorimetric detection offers an attractive visual detection approach for POC detection on low-cost paper-based microfluidic devices. Nevertheless, the sensitivity is low, and it is challenging for colorimetric detection to achieve quantitative analysis without the aid of other advanced equipment, reaching a bottleneck for the paper-based colorimetric assay to be widely used in practice. Third, microfluidic volumetric bar-chart chips[41−43] were designed as a high-degree integrative platform for visual quantitative detection based on the distance, where a color dye plug moves through a channel without using pneumatic pumps and signal collection devices. For example, Qin's group[44] reported an enzyme-linked immunosorbent assay (ELISA)-based competitive multiplexed volumetric bar-chart chip for the quantitative detection of small molecules, cancer biomarkers, and drug abuse screening. Moreover, using a "competition mode", a real-time internal control was embedded in the POC chip to decrease the potential influence of the background resulting in few false-negative or false-positive results. However, this platform still suffers three major drawbacks—the tedious and costly fabrication of glass chips, complex operation procedures, and temperature-sensitive enzymes employed as the catalysts—limiting their applications for resource-poor settings such as on-site or field detection.

Due to excellent catalysis performance and robustness at the ambient temperature for the on-site detection, various nanomaterials have been employed as catalysts in the POCTs.[45−47] Compared with traditional enzyme-based catalytic reactions, nanomaterials can provide more stable and efficient catalytic properties for signal amplification, such as higher sensitivity by versatile high-surface-to-volume-ratio nanostructures, higher robustness in a complex nonlab setting, and versatile functionalization via a controllable self-assembly or surface modification.[48−51] Numerous metallic[52−54] and carbon-based nanomaterials[55,56] were reported as highly sensitive catalysts for colorimetric,[57−59] chemiluminescent,[60,61] or electrochemical[62−64] detection. For instance, Yang's group[26] reported that platinum nanoparticles (PtNPs) generated more than 400 times O_2 per second than common catalase, resulting in much higher detection sensitivity than catalase methods. In addition, a new iron oxide-to-Prussian blue (PB) nanoparticle (NP) conversion strategy was developed and applied to sensitive colorimetric immunosensing of cancer biomarkers by Fu et al.[65] Utilizing the highly visible blue color change, this PB NPs-mediated colorimetric system can achieve a limit of detection (LOD) of 1.0 ng/mL for the prostate-specific antigen (PSA), with the LOD of about 80-fold lower than that of common gold nanoparticle (AuNP)-based colorimetric assays.

Herein, we developed a multiplexed (MB) bar-chart SpinChip integrated with nanomaterial-mediated aptasensors for visual quantitative instrument-free detection of multiple pathogens at the point of care, given the urgent demand for POCTs from pathogen detection and disease diagnosis. Three major foodborne pathogens, i.e., *Salmonella enterica* (*S. enterica*), *Escherichia coli* (*E. coli*), and *Listeria monocytogenes* (*L. monocytogenes*), were used as model analytes to demonstrate the method for the visual multiplexed quantitative analysis using the MB-SpinChip. These three kinds of foodborne bacteria commonly lead to a regional epidemic situation and serious emergencies, infecting about 1.2 million, 265 000, and 2500 persons per year by *Salmonella*, *E. coli,* and *Listeria* in the United States, respectively.[1] To the best of our knowledge, this is the first volumetric bar-chart chip for pathogen detection. Aptasensors can simply identify different types of pathogenic microorganisms specifically, eliminating complicated pathogen preparation steps. Nanoparticle-mediated pressure amplification utilized in the MB-SpinChip can not only amplify detection signals, but also enable the quantitative bar-chart readout from the MB-SpinChip. Additionally, on the basis of our recent work in a CD-like SpinChip for multiplexed loop-mediated DNA isothermal amplification (mLAMP),[30] we developed another spin unit on the MB-SpinChip, which not only provided convenient sample introduction from one inlet to multiple separate channels, but also gracefully solved the pressure cross-interference problem in the multiplexed volumetric bar-chart chip. Thus, our microfluidic platform does not need any specialized instruments for fluid manipulations or photo/electrosignal capturing devices, while maintaining the capacity for visual multiplexed quantitative analysis with high sensitivity, compared to other POC devices. Due to those significant features, our versatile MB-SpinChip can readily achieve simple quantitative sample-to-answer POC sensing in a multiplexed format in resource-limited settings.

EXPERIMENTAL SECTION

Reagents and Materials. All sequences of the three aptamers for *S. enterica*, *E. coli*, *L. monocytogenes* and their complementary DNA were synthesized from Integrated DNA Technologies (Coralville, IA), as listed in Table S-1. The DNA hybridization buffer (binding buffer) contained 50 mM Tris−HCl buffer, 5 mM KCl, 100 mM NaCl, and 1.0 mM $MgCl_2$ (pH 7.4). DNA stock solutions were prepared by ultrapure Milli-Q water (18.2 MΩ·cm) and stored at 4 °C with concentrations determined by a SpectraMax M3 from Molecular Devices, LLC (Sunnyvale, CA). Other common chemicals and materials are listed in the Supporting Information.

Layout and Fabrication of the MB-SpinChip. The pattern of each layer on the MB-SpinChip was designed with Adobe AI software and ablated on 2 mm thick poly(methyl

DOI: 10.1021/acs.analchem.8b02055
Anal. Chem. 2018, 90, 9888−9896

methacrylate) (PMMA) by a laser cutter from Epilog Laser (Golden, CO). As shown in Figures 1 and S-2, the MB-SpinChip consists of five patterned layers of PMMA. Compared to Figure 1, Figure S-2 also shows detailed specifications. The layer 1 sheet was designed in a flabellate shape (intersection angle, ∠134°) with one common sample inlet (dark green represents a hollow hole at the diameter of Φ = 1.2 mm by the laser vector process at 60% power and 10% speed) connected with four branched channels (light blue represents channels; dimensions, 15 mm × 0.3 mm, depth, 0.5 mm, by the laser raster process at 40% power and 30% speed), and four exhaust outlets (Φ = 0.7 mm). The layer 2 sheet was laser-ablated to create three inlets and two outlets for four parallel units, including the sample inlet, the substrate inlet, the indicator inlet, the exhaust outlet, and the bar-chart channel outlet. Accordingly, the layer 3 sheet includes four corresponding sets of microwells and channels for four parallel microfluidic units, including four sample recognition microwells (gold color; depth, 1.5 mm, by the laser raster process at 60% power and 20% speed), four catalytic amplification microwells (purple; depth, 1.5 mm), four indicator microwells (blue; depth, 1.5 mm), and four bar-chart channels (light green; depth, 0.5 mm). The channel width and depth of the microfluidic bar-chart channels were measured to be 387.7 ± 13.7 μm (RSD 3.5%) and 328.8 ± 9.4 μm (RSD 2.9%), respectively. Each amplification microwell is connected to a sample recognition microwell through a connection channel (red, 6 mm × 0.6 mm, 1.0 mm in depth, by the laser raster process at 50% power and 25% speed). A similar "T" phase-exchange channel (width, 0.3 mm; depth, 0.5 mm) was fabricated to keep the pressure balance while connecting three microwells. Three hollow circular microwells were fabricated at the bottom surface of the layer 4 sheet to hold circle magnets. The layer 5 sheet is the bottom layer to cover the magnet microwells. After the laser ablation process, the patterned layer 2 and layer 3 PMMA sheets were heat-bonded in an oven from VWR (Radnor, PA) at 150 °C for 60 min. The bonded layer 2−3 was hydrophobicated for 30 min by fully filling with fluorinated oil, which was evaporated in the air later. Afterward, 10 μL of the self-assembled DNA biosensor stock

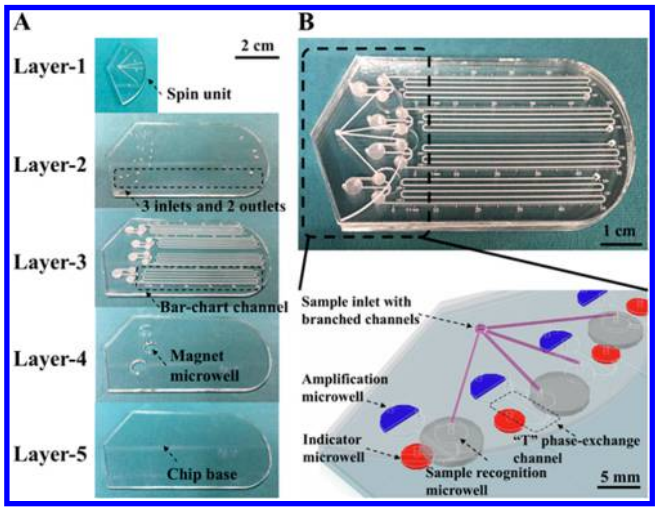

Figure 1. Exploded view (A) of the MB-SpinChip with five patterned PMMA sheets and (B) photograph and 3D schematic of an assembled MB-SpinChip. See more details of the MB-SpinChip from Figures S-2 and S-3.

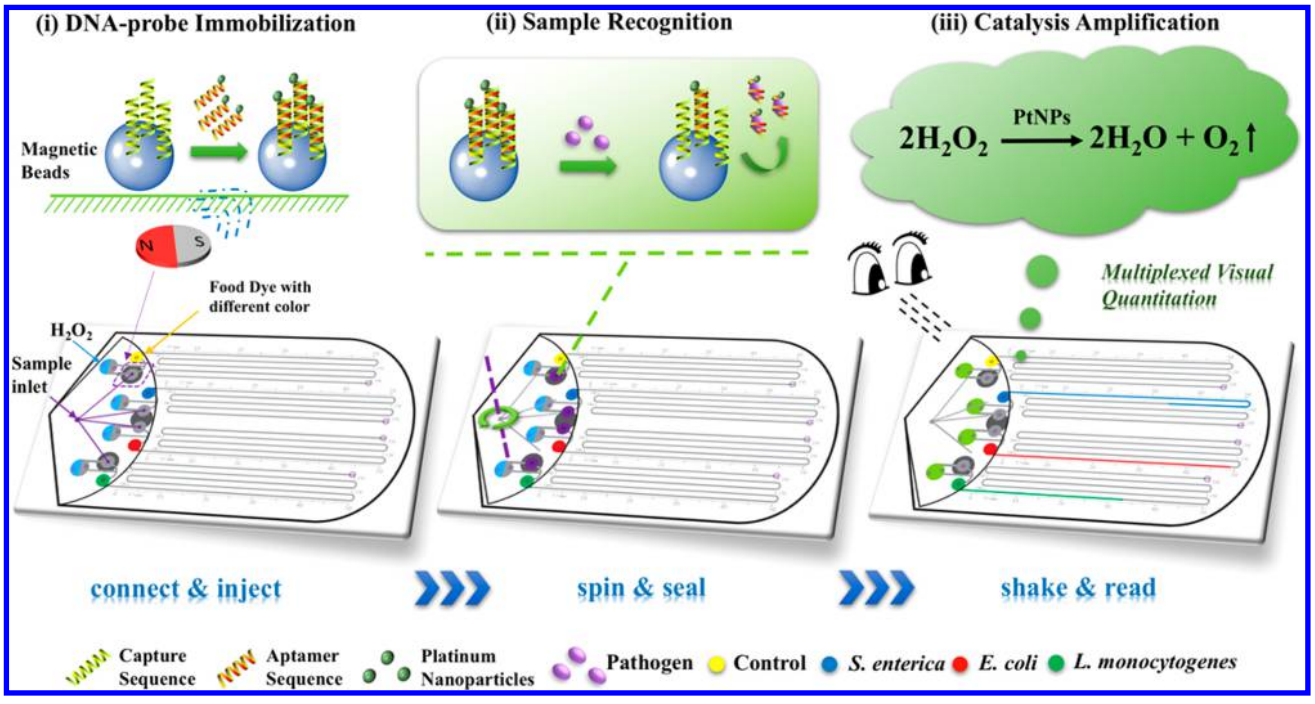

Figure 2. Schematic of the assay procedure. (i) DNA probe immobilization: H_2O_2 substrate solutions (light blue region), food dye solutions (yellow, dark blue, red, and green circle), and DNA probes (light gray circle) are, respectively, prestored in the MB-SpinChip. Herein, magnetic DNA probes are immobilized in different sample recognition microwells by a magnetic field (dark gray circle). (ii) Sample recognition: pathogens specifically combine with PtNPs−aptamers to form complexes which are then released into sample solutions (purple circle). (iii) Catalysis amplification: sample solutions and H_2O_2 solutions are mixed to generate O_2 with the pressure increase inside, resulting in the internal pressure increase which further leads to the food dye to move into channels to form different bar-chart signals for visual multiplexed pathogen detection.

DOI: 10.1021/acs.analchem.8b02055
Anal. Chem. 2018, 90, 9888−9896

solution was injected into the sample recognition microwell and kept in the vacuum desiccator to remove the solvent. Amounts of 10 μL of H_2O_2 and 10 μL of food dye were preinjected into the amplification microwell and the indicator microwell, respectively. The bonded layer 2−3, layer 4, and layer 5 PMMA sheets were easily assembled together by using super glue. The top layer 1 was tightened with the rest of the layers by a clamp, but could be manually rotated to set the spin unit to be "ON" or "OFF". Finally, the aptasensor-integrated MB-SpinChip was stored in a plastic zipper bag at 4 °C before use.

Other experimental sections that include the bacterial pathogen culture, the preparation of the DNA biosensor, and the assay procedure on the MB-SpinChip are listed in the Supporting Information.

RESULTS AND DISCUSSION

Working Principle of the MB-SpinChip for Visual Quantitative Multiplexed Detection. This MB-SpinChip is composed of four critical parts: spin unit, sample recognition unit, catalytic amplification unit, and bar-chart unit, as shown in Figures 1 and 2. The pattern of each unit was carefully optimized for full functionality. The spin unit is designed for efficient reagent delivery from one common inlet microwell to different sample recognition units, while the sample recognition unit and catalytic amplification are designed for pathogen recognition using the aptasensor and nanomaterial-mediated pressure amplification. An elaborate "T" phase-exchange channel is employed for the media exchange in a sealed condition, which guarantees the smooth interchange between the sample and the air in the amplification microwell after shaking. The bar-chart unit includes dye microwells, bar-chart channels with scale bars to provide the visual bar-chart signal readout. Figure 1A shows the exploded view of the MB-SpinChip, illustrating that three major layers (layers 1, 3, and 4) contain the spin unit, major bar-chart channels and reaction wells, and magnetic beads holders, respectively. Detailed specifications are shown in Figure S-2.

In order to measure multiple samples at a time in bar-chart microfluidics, multiple separate channels were often used for different analytes.[42,44] Because those channels were independent and separate sample injections were required for different analytes, those types of multiple sample assays lacked a high degree of integration, while a slight difference in sample injection can cause detection result variations after a manual slip. Using those glass-based reusable bar-chart slip-chips, several complicated operations have to be executed by trained personnel for the reagents injection, slip separation, and chip washing. In these cases, those bar-chart assays cannot be considered as genuine "sample-to-answer" by the sophisticated manual operations. Although it is not difficult for microfluidic methods to employ one inlet to introduce reagents to different locations just by adding a connection channel between a common inlet and different separate channels for reagent delivery, it will cause a pressure cross-interference issue for volume bar-chart chips, because generated gas can move freely in all those connected channels. Therefore, in this work we designed a spin unit to solve this issue, based on our recent work regarding a CD-shaped SpinChip for mLAMP.[30] The spin unit that we developed in this work is not only to deliver reagents, but also to disconnect each bar-chart channel by rotating the spin unit after the sample introduction step. More detailed principle of the MB-SpinChip is discussed in the following paragraph.

The working principle of the MB-SpinChip is composed of three main steps as illustrated in Figure 2, including (i) connect and inject, (ii) spin and seal, and (iii) shake and read. Before sample introduction, the nanoparticle-mediated magnetic DNA probe is assembled by DNA hybridization between magnetic-capture-beads−DNA (beads−DNA) and aptamer−DNA−platinum nanoparticles (aptamer−PtNPs). All synthetic and assembling processes are stated in the Experimental Section. The transmission electron microscopy (TEM) image in Figure S-1 shows the morphology of the synthesized PtNPs with a diameter of ∼4 nm. The assembled dual-nanoparticle conjugated DNA probe is preimmobilized in the sample recognition microwell by the magnetic field, which minimizes the complex chemical modification with the use of magnetism capturing. H_2O_2 and food dyes are also preinjected into the amplification microwell and the indicator microwell (see Figure S-3a), respectively. The MB-SpinChip then becomes ready to use. In step i, by rotating the spin unit, four parallel channels in the MB-SpinChip become connected with four sample recognition microwells, while keeping all exhaust outlets open. As such, the one-time sample injection allows the sample to be efficiently distributed into four sample recognition microwells (see Figure S-3b). In step ii, after sample introduction, all inlets and exhaust outlets are sealed by manually rotating the sectorial spin unit to disconnect separate bar-char channels with the common inlet, thus forming multiple hermetical reaction chambers (see Figure S-3c). Meanwhile, the sample recognition is initiated by mixing with the preloaded aptasensor after the sample injection. The sample containing pathogenic microorganisms reacts with the immobilized aptasensor to activate the specific binding reaction between the pathogen and aptamer−PtNPs to form the binding complexes. Under the magnetic field effect, the unreacted aptasensor is retained at the bottom of the sample recognition microwell, whereas the binding complexes become free in the solution. In step iii, by holding the right end of the MB-SpinChip, the binding complexes with PtNPs in parallel sample recognition microwells are shaken down into catalytic amplification microwells to mix with the H_2O_2 solution (see Figure S-3d). Oxygen gas (O_2) is generated quickly from H_2O_2 under the catalysis of PtNPs, causing a dramatic pressure increase in the sealed parallel chambers without interference from other chambers because of the "OFF" status of the spin unit. Thus, the pressure cross-interference problem in the multiplexed bar-chart chips is successfully addressed by the spin unit. High pressure will be transduced to the visual multiplexed bar-chart signal by driving different food dyes to move in different bar-chart channels. Because more pathogens result in higher pressure as indicated by a longer color dye bar-chart signal, the pathogen concentration is proportional to the moving distance of the dyes, achieving visual quantitative detection of pathogens. Likewise, different aptasensors in different detection units can be simultaneously applied in a single MB-SpinChip for multiplexed pathogen detection with high throughput. In the absence of the pathogen, the specific aptamer−PtNPs will not come off from the magnetic beads and stay in the recognition microwells due to the magnetic attraction. Hence, no O_2 generation reaction by the catalyst of PtNPs happens, following without noticeable bar-chart movement. Figure S-6 shows the whole assay procedure in detail.

DOI: 10.1021/acs.analchem.8b02055
Anal. Chem. 2018, 90, 9888−9896

We then conducted a series of experiments in the presence of different components of the aptasensor to demonstrate the feasibility of the proposed mechanism, while using *S. enterica* as the model pathogen. Four solutions with different DNA components were prepared for the visual bar-chart detection based on the MB-SpinChip. Solution a in the presence of only magnetic beads−DNA shows a negligible bar-chart signal (Figure 3A, part a). Because a few Fe_3O_4-nanoparticle beads

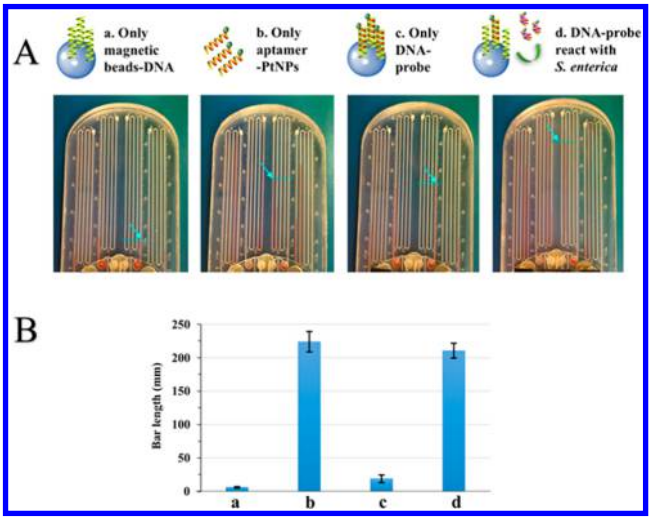

Figure 3. Photograph (A) and corresponding histogram of visual bar-chart (B) at different conditions: (a) only magnetic beads−DNA, (b) only PtNPs−aptamer, (c) only DNA probe, and (d) DNA probe reacting with *S. enterica*. The blue arrows and dotted lines indicate the end point of the dye bar and the quantitative values of scale marker, respectively. The standard deviation was obtained from four parallel measurements.

under the magnetic field were still shaken into the amplification microwell, a weak catalysis by Fe_3O_4-nanoparticle beads generated little O_2 and a short bar length. In the presence of only PtNPs−aptamer, a strong bar-chart signal of more than 200 mm was detected, due to the robust catalytic activity of PtNPs from the conjugated complex PtNPs−aptamer. However, when PtNPs−aptamer was hybridized on the magnetic beads forming the aptasensor probe, a much weaker bar-chart signal (less than 30 mm) was measured (Figure 3A, part c), which validated that the magnetic capturing is effective. The DNA hybridization could immobilize most PtNPs−aptamers, but a few nonhybridized PtNPs−aptamer were free in the solution and reacted with H_2O_2 forming a short bar length, which could be minimized as the background signal by optimizations. Once we had all the necessary components for the bar-chart assays including a pathogen sample and its specific aptasensor, a significant increase in the bar length was obtained with a mean value of 210 mm. It is much greater than the background result without the pathogen (mean value, 19 mm), implying the specific recognition and detection of the pathogen from the MB-SpinChip with the aptasensor. Taken together, our results clearly demonstrated the feasibility of our MB-SpinChip and that the nanoparticle-mediated magnetic aptasensor can recognize and bind with the pathogen to trigger a pressure catalytic amplification for the visual quantitative pathogen detection.

Condition Optimization and Selectivity of the MB-SpinChip. Several parameters were optimized for longer bar length against the background signal, namely, DNA probe washing times, the ratio of beads−DNA and PtNPs−aptamer, and the reaction time. To minimize the amount of unhybridized PtNPs−aptamers, we first optimized the DNA probe washing times on the MB-SpinChip. Figure 4A shows

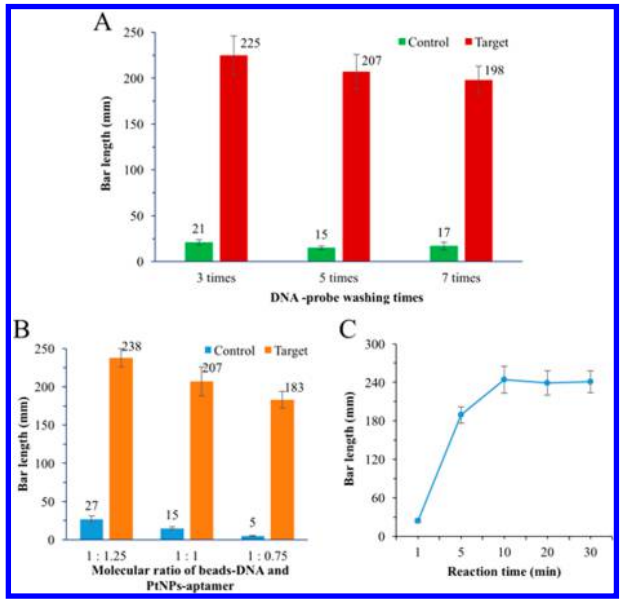

Figure 4. Optimization of (A) DNA probe washing times, (B) concentration ratio of beads−DNA and PtNPs−aptamer, and (C) the reaction time between DNA probes and pathogens. The error bars represent standard deviations from four parallel measurements.

different bar lengths in the presence of the target, *S. enterica*. The bar length decreased slightly with the increase of washing times from three to seven. Considering the biggest absolute increment between the target and the control, three times was selected as the optimal DNA probe washing times. Besides, the molecular ratio of beads−DNA and PtNPs−aptamer was optimized for the maximization of the target response increment against the control signal. As seen in Figure 4B, both the target and control signals increased with the increase of the ratios from 1:0.75 to 1:1.25 ([beads−DNA]/[PtNPs−aptamer]). The calculated bar length difference between the target and the control also increased with the increase of the ratio, reaching the maximum length at 1:1.25. Hence, the molecular ratio of 1:1.25 was chosen as the optimal molecular ratio of beads−DNA and PtNPs−aptamer. In addition, to ensure efficient binding between the DNA probe and the pathogen, the reaction time was optimized from 1 to 30 min. The bar length increased with the increase of the reaction time from 1 to 10 min, and then achieved a saturated level after 10 min (Figure 4C). Herein, 10 min was selected as the optimal reaction time between the DNA probe and the pathogen.

Considering the application of the MB-SpinChip in complex biological matrixes, the selectivity of three types of aptasensors targeting *S. enterica*, *E. coli*, and *L. monocytogenes* was evaluated using the MB-SpinChip. As shown in Figure 5, the *S. enterica* aptamer probe was used for the detection of 400 CFU/mL *S. enterica* and other pathogens at higher concentrations (more than 10^3-fold). Only the specific pathogen, the *S. enterica* sample, showed a long bar-chart signal of 162 mm, whereas the other two samples including *E. coli* and *L. monocytogenes* only showed very weak bar-chart signals of 30 mm, which was

DOI: 10.1021/acs.analchem.8b02055
Anal. Chem. 2018, 90, 9888−9896

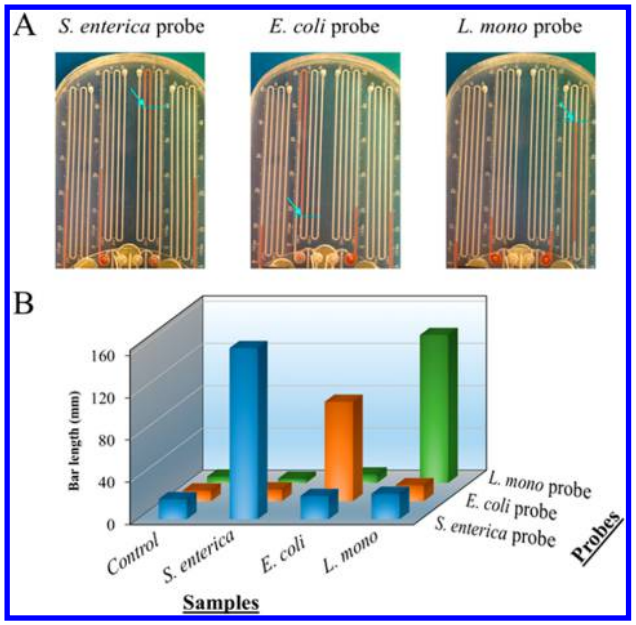

Figure 5. Selectivity investigation of the MB-SpinChip with different DNA probes for *S. enterica*, *E. coli*, and *L. monocytogenes* (abbreviated as *L. mono*) by their corresponding photographs (A) and bar-length histogram (B).

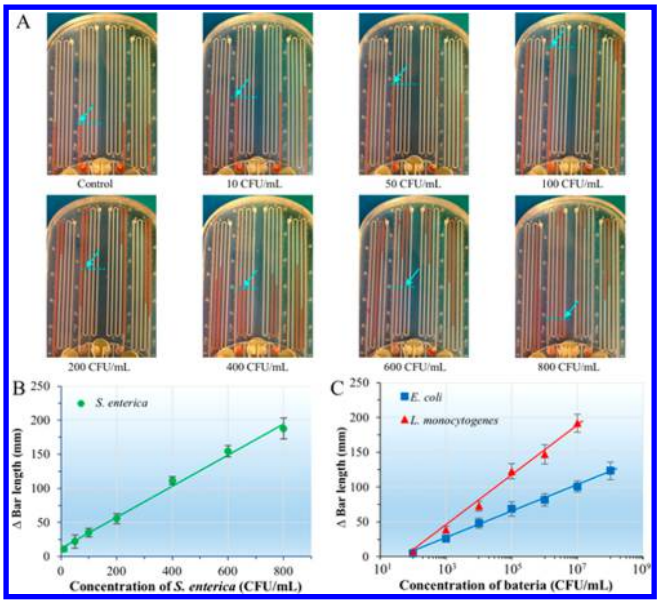

Figure 6. Visual quantitative pathogen detection using the MB-SpinChip. (A) Photographs of visual bar-chart responses to different concentrations of *S. enterica* from 10 to 800 CFU/mL. The blue arrows and dotted lines indicate the end point of the dye bars corresponding to different values on the scale bar. (B) Calibration curve of the bar-chart signal vs different concentrations of *S. enterica* (green line). (C) Calibration curves of the bar-chart signal vs different concentrations of *E. coli* from 10^2 to 10^8 CFU/mL (blue line) and *L. monocytogenes* from 10^2 to 10^7 CFU/mL (red line). The error bars represent standard deviations from four parallel measurements.

almost the same as the control experiment. Similarly, the *E. coli* aptasensor and *L. monocytogenes* aptasensor were also investigated with different pathogens. 10^6 CFU/mL *E. coli* and 10^6 CFU/mL *L. monocytogenes* gave bar-chart readings of 94 mm and 140 mm (see Figure S-4 in detail), respectively. On the contrary, the nonspecific pathogen samples at a higher concentration only showed a bar length of less than 20 mm. Therefore, the result confirmed the high specificity of our MB-SpinChip.

Visual Quantitative Detection of Pathogens. After optimization, the MB-SpinChip was first applied to visual quantitative detection of individual pathogens, *S. enterica*, *E. coli*, and *L. monocytogenes*. *S. enterica* was tested at various concentrations, with four parallel measurements using the MB-SpinChip. As shown in Figure 6A, the visual bar-chart signal increased with the increase of the concentration of *S. enterica* from 0 to 800 CFU/mL. Taking the length of the 0 CFU/mL of *S. enterica* as the blank, the Δlength between the target to the blank lengths of different concentrations of *S. enterica* was calculated and plotted versus the concentration. An excellent linear relationship between the mean Δlength and the *S. enterica* concentration was obtained in the range of 10−800 CFU/mL with the R^2 value of 0.994 (Figure 6B). The LOD of 6.7 CFU/mL *S. enterica* was achieved based on 3-folds of the standard deviation (SD) above the blank value. Compared with other POCTs for the detection of *S. enterica*, our instrument-free method has higher detection sensitivity than the SERS-based lateral flow strip (LOD, 27 CFU/mL)[66] and the colorimetric method (LOD, 100 CFU/mL)[67] using the UV−vis absorption spectrum. The sensitivity of our method is even comparable to that of DNA amplification-based lateral flow devices with the LOD of 4 CFU/mL.[68]

Following a similar protocol, different concentrations of *E. coli* and *L. monocytogenes* were separately tested by their corresponding aptasensors on the MB-SpinChip, and their absolute bar-chat differences are plotted in Figure 6C. It can be seen that the calibration curves for *E. coli* and *L. monocytogenes* were linearly fitted in the range from 10^2 to 10^8 CFU/mL (R^2 = 0.996) and 10^2−10^7 CFU/mL (R^2 = 0.995), respectively. The LOD values of *E. coli* and *L. monocytogenes* are 16 and 20 CFU/mL, respectively. Even compared with other DNA amplification methods, the sensitivity of our method is better than the LOD of 100 CFU/mL for *E. coli* by a LAMP method with electrochemical impedance detection[69] and comparable to the LOD of 10 CFU/mL for *L. monocytogenes* by a polymerase chain reaction (PCR) method with electrochemiluminescence-based gene sensing.[70] These results indicate high detection sensitivities of our bar-chart SpinChip for visual quantitative detection of multiple pathogens and lay a solid foundation for us to explore its capacity in the subsequent multiplexed pathogen detection.

Multiplexed Quantitative Detection and Validation Using Spiked Juice Samples. As multiple pathogens can coexist, multiplexed detection becomes increasingly important, especially in testing complex biological samples and unknown samples.[71−74] The multiplexed measurement can not only enhance the throughput and convenience for higher detection efficiency, but also provide richer information at lower cost from a single assay.[30] Since the spin unit solved a major issue in multiplexed bar-chart microfluidics, multiple aptasensors were simultaneously integrated in one MB-SpinChip for multiplexed detection of various pathogens. Herein, *S. enterica*, *E. coli*, and *L. monocytogenes* were chosen as a complex model of foodborne diseases. We first injected different aptamer probes into different sample recognition microwells and four different food dyes into four indicator microwells to distinguish different targets. Then, after three different aptasensors were integrated on the same bar-chart chips, the multiplexed SpinChips were first used to test individual targets. As shown

DOI: 10.1021/acs.analchem.8b02055
Anal. Chem. 2018, 90, 9888−9896

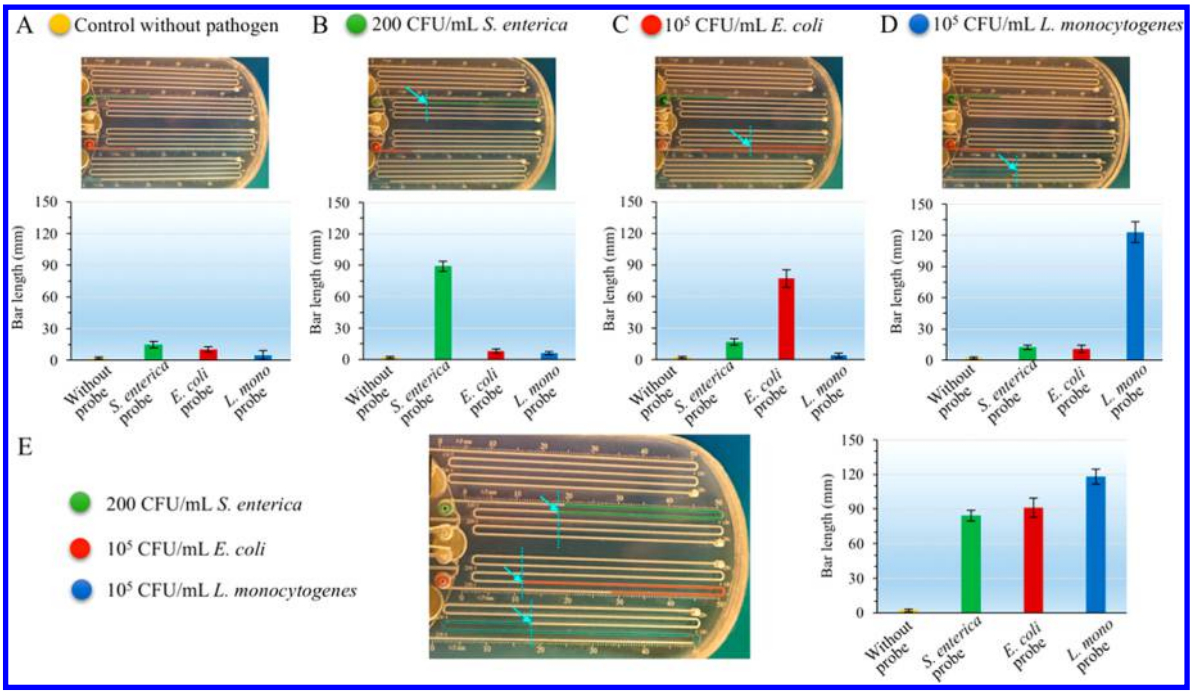

Figure 7. Multiplexed pathogen detection. (A) Control without pathogens on the MS-SpinChip. (B–D) Testing individual pathogens using the MS-SpinChip: (B) 200 CFU/mL *S. enterica*, (C) 10^5 CFU/mL *E. coli*, (D) 10^5 CFU/mL *L. monocytogenes* (abbreviated as *L. mono*). (E) Simultaneous detection of three types of pathogens on a single MB-SpinChip. The pathogen concentrations in panel E correspond to the same concentrations in panels B–D, respectively. The yellow bar, green bar, red bar, and blue bar represent the control signal, *S. enterica* signal, *E. coli* signal, and *L. mono* signal, respectively.

Table 1. Detection of Multiple Pathogens Spiked in Apple Juice Samples[a]

pathogen	spiked concn (CFU/mL)	av measurement ± SD (CFU/mL)	CV (%)	recovery (%)
S. enterica	50	51.64 ± 3.14	6.08	103.29
	100	95.84 ± 8.75	9.13	95.84
E. coli	1.0×10^3	$(1.08 \pm 0.095) \times 10^3$	8.77	108.40
	1.0×10^4	$(1.00 \pm 0.095) \times 10^4$	9.48	100.41
L. monocytogenes	1.0×10^3	$(0.98 \pm 0.069) \times 10^3$	7.03	98.90
	1.0×10^4	$(0.96 \pm 0.068) \times 10^4$	7.07	96.53

[a]Standard deviations (SDs) and coefficients of variation (CVs) were obtained from four parallel measurements.

in Figure 7, sample A without any pathogens (the negative control) was measured and only showed weak background bar-chart signals. Because the concentrations of different aptamer probes were optimized for higher sensitivity to corresponding pathogens, slightly different background signals were observed when testing the same mixture using different aptasensors. However, all the negative control signals were below 20 mm. But when sample B including 200 CFU/mL *S. enterica* was detected using the MB-SpinChip integrated with three aptasensors, there was a significant increase in the green bar to 89 mm, while no other color bars were observed, as indicated by the bar-chart graph in Figure 7B. Similarly, sample C including 10^5 CFU/mL *E. coli* and sample D including 10^5 CFU/mL *L. monocytogenes* were separately tested by using different MB-SpinChips. Parts C and D of Figure 7 indicated dramatic bar-chart signal increases of 77 mm in the red bar (i.e., *E. coli*) and 123 mm in the blue bar (*L. monocytogenes*), with no noticeable increases of other color bars. These results confirmed that individual pathogens could be effectively and quantitatively detected by the MB-SpinChip, when different aptasensors were integrated on the same bar-chart chips.

The multiplexed detection capacity was further tested by simultaneously detecting three types of pathogens that coexisted in one sample using our multiplexed bar-chart SpinChip. As shown in Figure 7E, when 200 CFU/mL *S. enterica*, 10^5 CFU/mL *E. coli*, and 10^5 CFU/mL *L. monocytogenes* from a single injection were detected on the same chip, their corresponding bar-chart channels showed strong signals, i.e., a 84 mm green bar, a 91 mm red bar, and a 118 mm blue bar, respectively. Their bar lengths of sample E in the simultaneous detection are consistent with their corresponding values tested in samples B, C, and D in the presence of only one pathogen in each sample. Hence, this further confirmed the strong multiplexing capacity of our MB-SpinChip in the visual quantitative detection of multiple pathogens simultaneously, without the aid of any equipment.

To validate our MB-SpinChip in multiplexed detection, a food sample, apple juice, was spiked with *S. enterica*, *E. coli*, and *L. monocytogenes*, and the pathogens were simultaneously measured using our MB-SpinChips. As listed in Table 1, all the recovery values from the different pathogens were determined at the satisfactory level between 95% and 110%, and all the coefficients of variation (CVs) are <10%. Consequently, the aptasensor-integrated MB-SpinChip can be effectively applied for the multiplexed detection of pathogens in food samples.

DOI: 10.1021/acs.analchem.8b02055
Anal. Chem. 2018, 90, 9888–9896

CONCLUSION

In summary, we have developed a portable, low-cost, and instrument-free multiplexed bar-chart SpinChip integrated with PtNPs-mediated magnetic aptasensor for the visual quantitative and simultaneous detection of multiple pathogens. We used *S. enterica* as a model to develop the MB-SpinChip, and then successfully extended to the multiplexed detection of three pathogens, *S. enterica*, *E. coli*, and *L. monocytogenes*, in which the newly developed spin unit played a crucial role in the multiplexed bar-chart chip. Three major types of foodborne pathogens were quantified simultaneously using the MB-SpinChip with high detection sensitivity. LODs of about 10 CFU/mL were readily achieved, without using any equipment. Additionally, compared to other glass or glass/polymer based bar-chart V-chips, our multiplexed bar-chart SpinChip does not (1) need sophisticated operation procedures,[41,43] and (2) complicated and costly photolithography and chemical etching in other bar-chart chip fabrication, (3) the PMMA substrate allows lower cost and more environmentally friendly bioassays, compared to glass-based bar-chart chips, and (4) nanoparticle-mediated catalysis is not as sensitive to ambient temperatures as enzymes which were commonly used in other bar-chart chips.[44,75]

Multiple important features of the MB-SpinChip are appealing as a universal POC platform for the multiplexed detection of pathogens and other biochemicals. (i) The visual quantitative detection can be achieved without using any specialized instrument. Instead of relying on complicated pneumatic pumps and expensive signal detectors, PtNPs-mediated catalytic pressure amplification integrated on the MB-SpinChip provides a robust driving force to transduce the pressure signal into visual dye bar charts. A user-friendly quantitative bar-chart readout can be conducted on the MB-SpinChip similarly to a traditional thermometer. (ii) Multiplexed detection of multiple pathogens can be accomplished from a single assay. By integrating the innovative spin unit on the MB-SpinChip, we can readily deliver reagents and samples from one inlet to different channels without causing pressure cross-interference problems during the subsequent detection step. When integrated with multifarious aptasensors, simultaneous measurements of multiple pathogens can be efficiently completed on a single MB-SpinChip at a time. (iii) The method owns high simplicity. Our method utilizes specific aptasensors to recognize bacterial microorganisms directly, without the need of cell lysis and other complicated sample preparation procedures. (iv) The PtNPs-mediated magnetic aptasensor-integrated MB-SpinChip has great potential and wide applications in the POC detection of a wide range of pathogens and biochemicals in food safety, environment surveillance, and infectious disease diagnosis at the point of care and other low-resource settings.

ASSOCIATED CONTENT

Supporting Information

The Supporting Information is available free of charge on the ACS Publications website at DOI: 10.1021/acs.analchem.8b02055.

Detailed information on the reagents and materials, some assays (PDF)

AUTHOR INFORMATION

Corresponding Author

*E-mail: xli4@utep.edu.

ORCID

Xiaofeng Wei: 0000-0002-1341-8938
Qijie Jin: 0000-0002-3853-7968
Feng Xu: 0000-0003-4351-0222
XiuJun Li: 0000-0002-7954-0717

Notes

The authors declare no competing financial interest.

ACKNOWLEDGMENTS

We would like to acknowledge the financial support from the National Institute of Allergy and Infectious Disease of the NIH (R21AI107415), the National Institute of General Medical Sciences of the NIH (SC2GM105584), and the U.S. NSFPREM program (DMR 1205302). Financial support from the NIH RCMI Pilot Grant, the Emily Koenig Meningitis Fund of the Philadelphia Foundation, the Medical Center of the Americas Foundation, the NIH BUILDing Scholar Summer Sabbatical Award (NIGMS Award Nos. RL5GM118969, TL4GM118971, and UL1GM11897), the University of Texas at El Paso (UTEP) for the IDR Program, and University of Texas (UT) System for the STARS award is also greatly acknowledged.

REFERENCES

(1) *Who Estimates of the Global Burden of Foodborne Diseases*. Foodborne Diseases Burden Epidemiology Reference Group 2007−2015; WHO: Geneva, Switzerland, 2015.

(2) Kim, J. Y.; Sahu, S.; Yau, Y. H.; Wang, X.; Shochat, S. G.; Nielsen, P. H.; Dueholm, M. S.; Otzen, D. E.; Lee, J.; Delos Santos, M. M. S.; Yam, J. K. H.; Kang, N. Y.; Park, S. J.; Kwon, H.; Seviour, T.; Yang, L.; Givskov, M.; Chang, Y. T. *J. Am. Chem. Soc.* **2016**, *138*, 402−407.

(3) Ruehle, B.; Clemens, D. L.; Lee, B. Y.; Horwitz, M. A.; Zink, J. I. *J. Am. Chem. Soc.* **2017**, *139*, 6663−6668.

(4) Xiong, L. H.; Cui, R.; Zhang, Z. L.; Yu, X.; Xie, Z. X.; Shi, Y. B.; Pang, D. W. *ACS Nano* **2014**, *8*, 5116−5124.

(5) Safavieh, M.; Pandya, H. J.; Venkataraman, M.; Thirumalaraju, P.; Kanakasabapathy, M. K.; Singh, A.; Prabhakar, D.; Chug, M. K.; Shafiee, H. *ACS Appl. Mater. Interfaces* **2017**, *9*, 12832−12840.

(6) Liu, H. X.; Zhou, X. M.; Liu, W. P.; Yang, X. K.; Xing, D. *Anal. Chem.* **2016**, *88*, 10191−10197.

(7) Daggumati, P.; Appelt, S.; Matharu, Z.; Marco, M. L.; Seker, E. *J. Am. Chem. Soc.* **2016**, *138*, 7711−7717.

(8) Wang, S. Q.; Deng, W. F.; Yang, L.; Tan, Y. M.; Xie, Q. J.; Yao, S. Z. *ACS Appl. Mater. Interfaces* **2017**, *9*, 24440−24445.

(9) Carey, J. R.; Suslick, K. S.; Hulkower, K. I.; Imlay, J. A.; Imlay, K. R. C.; Ingison, C. K.; Ponder, J. B.; Sen, A.; Wittrig, A. E. *J. Am. Chem. Soc.* **2011**, *133*, 7571−7576.

(10) Bui, M. P. N.; Ahmed, S.; Abbas, A. *Nano Lett.* **2015**, *15*, 6239−6246.

(11) Granger, J. H.; Schlotter, N. E.; Crawford, A. C.; Porter, M. D. *Chem. Soc. Rev.* **2016**, *45*, 3865−3882.

(12) Van Lierop, D.; Larmour, I. A.; Faulds, K.; Graham, D. *Anal. Chem.* **2013**, *85*, 1408−1414.

(13) Kwon, D.; Joo, J.; Lee, J.; Park, K. H.; Jeon, S. *Anal. Chem.* **2013**, *85*, 7594−7598.

(14) Martinez, A. W.; Phillips, S. T.; Whitesides, G. M.; Carrilho, E. *Anal. Chem.* **2010**, *82*, 3−10.

(15) Fu, G. L.; Sanjay, S. T.; Dou, M. W.; Li, X. J. *Nanoscale* **2016**, *8*, 5422−5427.

(16) Wei, X.; Tian, T.; Jia, S.; Zhu, Z.; Ma, Y.; Sun, J.; Lin, Z.; Yang, C. J. *Anal. Chem.* **2015**, *87*, 4275−4282.

DOI: 10.1021/acs.analchem.8b02055
Anal. Chem. 2018, 90, 9888−9896

(17) Shin, J. H.; Hong, J.; Go, H.; Park, J.; Kong, M.; Ryu, S.; Kim, K.; Roh, E.; Park, J. K. *J. Agric. Food Chem.* **2018**, *66*, 290−297.
(18) Ma, X. M.; Chen, Z. T.; Kannan, P.; Lin, Z. Y.; Qiu, B.; Guo, L. H. *Anal. Chem.* **2016**, *88*, 3227−3234.
(19) Fu, G. L.; Sanjay, S. T.; Li, X. J. *Analyst* **2016**, *141*, 3883−3889.
(20) Sanjay, S. T.; Dou, M.; Sun, J.; Li, X. *Sci. Rep.* **2016**, *6*, 30474.
(21) Yan, L.; Zhu, Z.; Zou, Y.; Huang, Y.; Liu, D.; Jia, S.; Xu, D.; Wu, M.; Zhou, Y.; Zhou, S.; Yang, C. J. *J. Am. Chem. Soc.* **2013**, *135*, 3748−3751.
(22) Gu, C. M.; Lan, T.; Shi, H. C.; Lu, Y. *Anal. Chem.* **2015**, *87*, 7676−7682.
(23) Zhang, J. J.; Shen, Z.; Xiang, Y.; Lu, Y. *ACS Sensors* **2016**, *1*, 1091−1096.
(24) Zhu, X.; Kou, F. X.; Xu, H. F.; Lin, L. P.; Yang, G. D.; Lin, Z. Y. *Sens. Actuators, B* **2017**, *253*, 660−665.
(25) Wang, Q.; Li, R.; Shao, K.; Lin, Y.; Yang, W.; Guo, L.; Qiu, B.; Lin, Z.; Chen, G. *Sci. Rep.* **2017**, *7*, 45343.
(26) Zhu, Z.; Guan, Z. C.; Liu, D.; Jia, S. S.; Li, J. X.; Lei, Z. C.; Lin, S. C.; Ji, T. H.; Tian, Z. Q.; Yang, C. Y. J. *Angew. Chem., Int. Ed.* **2015**, *54*, 10448−10453.
(27) Liu, D.; Jia, S.; Zhang, H.; Ma, Y.; Guan, Z.; Li, J.; Zhu, Z.; Ji, T.; Yang, C. J. *ACS Appl. Mater. Interfaces* **2017**, *9*, 22252−22258.
(28) Zhang, L.; Ding, B.; Chen, Q.; Feng, Q.; Lin, L.; Sun, J. *TrAC, Trends Anal. Chem.* **2017**, *94*, 106−116.
(29) Zhang, L.; Tian, F.; Liu, C.; Feng, Q.; Ma, T.; Zhao, Z.; Li, T.; Jiang, X.; Sun, J. *Lab Chip* **2018**, *18*, 610−619.
(30) Dou, M.; Sanjay, S. T.; Dominguez, D. C.; Zhan, S.; Li, X. J. *Chem. Commun.* **2017**, *53*, 10886−10889.
(31) Dou, M.; Dominguez, D. C.; Li, X.; Sanchez, J.; Scott, G. *Anal. Chem.* **2014**, *86*, 7978−7986.
(32) Fu, G.; Sanjay, S. T.; Zhou, W.; Brekken, R. A.; Kirken, R. A.; Li, X. *Anal. Chem.* **2018**, *90*, 5930.
(33) Liu, H.; Crooks, R. M. *J. Am. Chem. Soc.* **2011**, *133*, 17564−17566.
(34) Deng, X. D.; Smeets, N. M. B.; Sicard, C.; Wang, J. Y.; Brennan, J. D.; Filipe, C. D. M.; Hoare, T. *J. Am. Chem. Soc.* **2014**, *136*, 12852−12855.
(35) Glavan, A. C.; Niu, J.; Chen, Z.; Guder, F.; Cheng, C. M.; Liu, D.; Whitesides, G. M. *Anal. Chem.* **2016**, *88*, 725−731.
(36) Phillips, S. T.; Lewis, G. G. *Expert Rev. Mol. Diagn.* **2014**, *14*, 123−125.
(37) Lewis, G. G.; Robbins, J. S.; Phillips, S. T. *Anal. Chem.* **2013**, *85*, 10432−10439.
(38) Baker, M. S.; Phillips, S. T. *J. Am. Chem. Soc.* **2011**, *133*, 5170−5173.
(39) Jeong, S. G.; Lee, S. H.; Choi, C. H.; Kim, J.; Lee, C. S. *Lab Chip* **2015**, *15*, 1188−1194.
(40) Lewis, G. G.; DiTucci, M. J.; Phillips, S. T. *Angew. Chem., Int. Ed.* **2012**, *51*, 12707−12710.
(41) Song, Y.; Zhang, Y.; Bernard, P. E.; Reuben, J. M.; Ueno, N. T.; Arlinghaus, R. B.; Zu, Y.; Qin, L. *Nat. Commun.* **2012**, *3*, 1283.
(42) Zhu, Z.; Guan, Z.; Jia, S.; Lei, Z.; Lin, S.; Zhang, H.; Ma, Y.; Tian, Z. Q.; Yang, C. J. *Angew. Chem., Int. Ed.* **2014**, *53*, 12503−12507.
(43) Song, Y.; Wang, Y.; Qin, L. *J. Am. Chem. Soc.* **2013**, *135*, 16785−16788.
(44) Li, Y.; Xuan, J.; Xia, T.; Han, X.; Song, Y.; Cao, Z.; Jiang, X.; Guo, Y.; Wang, P.; Qin, L. *Anal. Chem.* **2015**, *87*, 3771−3777.
(45) Zhou, W.; Gao, X.; Liu, D.; Chen, X. *Chem. Rev.* **2015**, *115*, 10575−10636.
(46) Zhu, C.; Yang, G.; Li, H.; Du, D.; Lin, Y. *Anal. Chem.* **2015**, *87*, 230−249.
(47) Tang, L.; Li, J. *ACS Sensors* **2017**, *2*, 857−875.
(48) Farka, Z.; Jurik, T.; Kovar, D.; Trnkova, L.; Skladal, P. *Chem. Rev.* **2017**, *117*, 9973−10042.
(49) Mistry, H.; Varela, A. S.; Kuhl, S.; Strasser, P.; Cuenya, B. R. *Nat. Rev. Mater.* **2016**, *1*, 16009.
(50) Ge, S.; Zhang, L.; Zhang, Y.; Lan, F.; Yan, M.; Yu, J. *Nanoscale* **2017**, *9*, 4366−4382.
(51) Liu, D.; Tian, T.; Chen, X.; Lei, Z.; Song, Y.; Shi, Y.; Ji, T.; Zhu, Z.; Yang, L.; Yang, C. *Analyst* **2018**, *143*, 1294−1304.
(52) Li, J.-F.; Zhang, Y.-J.; Ding, S.-Y.; Panneerselvam, R.; Tian, Z.-Q. *Chem. Rev.* **2017**, *117*, 5002−5069.
(53) Chen, H. M.; Liu, R. S. *J. Phys. Chem. C* **2011**, *115*, 3513−3527.
(54) Sethi, M.; Pacardo, D. B.; Knecht, M. R. *Langmuir* **2010**, *26*, 15121−15134.
(55) Shen, K.; Chen, X. D.; Chen, J. Y.; Li, Y. W. *ACS Catal.* **2016**, *6*, 5887−5903.
(56) Hu, M. C.; Yao, Z. H.; Wang, X. Q. *Ind. Eng. Chem. Res.* **2017**, *56*, 3477−3502.
(57) Thiramanas, R.; Jangpatarapongsa, K.; Tangboriboonrat, P.; Polpanich, D. *Anal. Chem.* **2013**, *85*, 5996−6002.
(58) Li, H.; Liu, H.; Zhang, J.; Cheng, Y.; Zhang, C.; Fei, X.; Xian, Y. *ACS Appl. Mater. Interfaces* **2017**, *9*, 40716−40725.
(59) Ye, X.; Shi, H.; He, X.; Wang, K.; He, D.; Yan, L.; Xu, F.; Lei, Y.; Tang, J.; Yu, Y. *Anal. Chem.* **2015**, *87*, 7141−7147.
(60) Wang, J.; Zhong, W.; Liu, X.; Yang, T.; Li, F.; Li, Q.; Cheng, W.; Gao, C.; Jiang, Z.; Jiang, J.; Cui, H. *Anal. Chem.* **2017**, *89*, 13518−13523.
(61) Wang, X.; Na, N.; Zhang, S.; Wu, Y.; Zhang, X. *J. Am. Chem. Soc.* **2007**, *129*, 6062−6063.
(62) Bas, S. Z.; Cummins, C.; Borah, D.; Ozmen, M.; Morris, M. A. *Anal. Chem.* **2018**, *90*, 1122−1128.
(63) Chen, A.; Ostrom, C. *Chem. Rev.* **2015**, *115*, 11999−12044.
(64) Lv, H.; Xi, Z.; Chen, Z.; Guo, S.; Yu, Y.; Zhu, W.; Li, Q.; Zhang, X.; Pan, M.; Lu, G.; Mu, S.; Sun, S. *J. Am. Chem. Soc.* **2015**, *137*, 5859−5862.
(65) Fu, G.; Sanjay, S. T.; Li, X. *Analyst* **2016**, *141*, 3883−3889.
(66) Liu, H. B.; Du, X. J.; Zang, Y. X.; Li, P.; Wang, S. *J. Agric. Food Chem.* **2017**, *65*, 10290−10299.
(67) Lavu, P. S.; Mondal, B.; Ramlal, S.; Murali, H. S.; Batra, H. V. *ACS Comb. Sci.* **2016**, *18*, 292−301.
(68) Xu, Y.; Wei, Y.; Cheng, N.; Huang, K.; Wang, W.; Zhang, L.; Xu, W.; Luo, Y. *Anal. Chem.* **2018**, *90*, 708−715.
(69) Tlili, C.; Sokullu, E.; Safavieh, M.; Tolba, M.; Ahmed, M. U.; Zourob, M. *Anal. Chem.* **2013**, *85*, 4893−4901.
(70) Zhu, M.; Liu, W.; Liu, H.; Liao, Y.; Wei, J.; Zhou, X.; Xing, D. *ACS Appl. Mater. Interfaces* **2015**, *7*, 12873−12881.
(71) Rusling, J. F. *Anal. Chem.* **2013**, *85*, 5304−5310.
(72) Sanjay, S. T.; Fu, G. L.; Dou, M. W.; Xu, F.; Liu, R. T.; Qi, H.; Li, X. J. *Analyst* **2015**, *140*, 7062−7081.
(73) Du, W.; Li, L.; Nichols, K. P.; Ismagilov, R. F. *Lab Chip* **2009**, *9*, 2286−2292.
(74) Zuo, P.; Li, X.; Dominguez, D. C.; Ye, B. C. *Lab Chip* **2013**, *13*, 3921−3928.
(75) Cate, D. M.; Dungchai, W.; Cunningham, J. C.; Volckens, J.; Henry, C. S. *Lab Chip* **2013**, *13*, 2397−2404.

DOI: 10.1021/acs.analchem.8b02055
Anal. Chem. 2018, 90, 9888−9896